Direct Observation of Interactions between Individual Atoms on Tungsten Surfaces*

Tien Tzou Tsong
Department of Physics, The Pennsylvania State University, University Park, Pennsylvania 16802
(Received 2 February 1972)

Using the field ion microscope (FIM), it is possible to investigate the interactions between individual atoms on metal surfaces. The number of atoms participating in an experiment can be specified and controlled by successive depositions or field evaporations. It is found that the interaction potential between two atoms depends on the substrate surface structure. In agreement with other investigators, the binding energy is found to be not pairwise additive. The interatomic potential between two Re atoms on W (110) planes shows at least two minima and a maximum, suggesting an oscillatory structure similar to the well-known Friedel oscillation. Surface migration as well as structures of clusters with less than six atoms is also investigated. It is found that the equilibrium structures of the clusters depend very sensitively on surface temperature. It is also found that potential traps of ~ 0.14 eV exist on crystal planes which otherwise appear to be perfectly regular in the FIM images.

I. INTRODUCTION

A metal atom on a surface plane interacts with its environment in many ways. It is bound to the substrate lattice with a binding energy of several eV. At higher temperatures, the surface atom may start to migrate before the dissolution of the substrate plane. On its diffusion path, the atom may be trapped into a potential well resulting from an impurity atom or lattice defects either on or beneath the surface plane. The diffusing atom may also encounter another atom and interact with it, either by combining with it or repelling it. By tracing the movement of an atom on a surface plane and observing its interaction with other atoms, information on the surface-potential profile as well as the interatomic potential between two atoms on the surface plane may be deduced. An understanding of the various interactions is of interest to crystal growth, catalysis, solid state and surface theories, and also in its own right. The field ion microscope (FIM),[1] with its atomic resolution, is most suitable for investigating the atomic processes on metal surfaces at an atomic scale. Müller[2] first realized the possibility of studying surface diffusion as well as determining the binding energies of individual atoms on various crystal planes. Ehrlich and Hudda's[3] work on atomic view of surface diffusion represents the first individual-atom experiment where quantitative information has been obtained. Since then a number of individual-atom experiments have been carried out and useful results gained. References 3–8 are some of the works related to the present investigations. Here we shall discuss our experiments on surface diffusion of rhenium atoms, on interaction between two rhenium atoms and various combinations of rhenium and tungsten atoms, and also on formation and diffusion as well as structures of multiatomic clusters. All the results were obtained with thermally deposited atoms on field evaporated tungsten surfaces. In contrast to all other individual-atom works, the number of atoms participating in our experiment was specified beforehand and was then carefully controlled by repeated depositions combined with dc or pulsed-field evaporations.

II. EXPERIMENTAL TECHNIQUES

The microscope system as well as its operation procedures can be found elsewhere.[1] A bakeable, glass, ultrahigh-vacuum FIM with two side arms was used in the present work. Each side arm was equipped with four leads, two for heating the deposition wire source and two for degassing the leads. The deposition sources are 0.004-in. tungsten and rhenium coils, respectively. They are kept ~15 mm away from the tip.

The tip temperature is controlled by passing a dc heating current, supplied from a constant-current power supply, through a 0.004-in. Pt tip-mounting loop. Two 0.001-in. Pt wires, spot welded on the loop, serve as potential leads for temperature monitoring. Both the heating current and the potential are measured with an accurate digital voltmeter. Temperature calibration was carried out with the system itself before an experimental run. Each heating cycle is 3 min. The tip temperature takes 35 sec to reach 95% of its equilibrium value. The heating time for each cycle is therefore taken to be 145 sec. The calibration is quite precise and reproducible. The accuracy is probably around ±5 K.

As in any other individual-atom experiment, the cleanliness of the emitter surface under the heating cycles is essential in obtaining meaningful results. In our system, after 24-h baking and careful degassing, a vacuum well under 10^{-10} Torr is easily achieved. Before the system is cut off from diffusion pumps by a mercury cutoff value with two

cold traps in series, the deposition sources are thoroughly degassed at deposition temperatures, the tip is degassed at ~ 800 °C for 60 sec, the helium-admitting Vycor-glass bulb is heated to 500 °C for 5 min and a titanium getter is fully activated. Helium gas of pressure 2.0 mTorr is then diffused through the bulb into the system at ~ 350 °C. With this treatment, even after the system has been closed off for several hours and going through more than 60 heating cycles up to 450 K, no contamination of a single image spot can be detected by turning the imaging voltage off for 5 min. When we are performing experiments with one or a few atoms for several hours and tens of heating cycles, it is essential that we are perfectly sure whether an accidental field evaporation of atoms occurred. Thus after each heating cycle, when the imaging voltage is slowly raised, a very careful visual observation is mandatory. Our choice of tungsten and rhenium adatoms insures us a visual detection of any accidental field evaporation.

All the micrographs shown were taken with liquid-nitrogen cooling of the specimen. The location of adatoms as well as their displacements after each heating cycle can be determined by Müller's color-superposition technique.[1] In our case we found it more convenient to trace the image contour of crystal planes or atomic rows of interest as well as the positions of adatoms on a paper with a microprojector. By means of fiduciary marks, internal (e.g., image of lattice atoms in well-resolved planes or zone-line decoration atoms) or external, the center of a given image point can be accurately determined. In fact the displacements of an adatom can be determined to an accuracy of 0.5 Å, better than the 3-Å resolution of the FIM (the resolution is the ability of the FIM to image two atoms as separate image points).

III. ATOMIC VIEW OF SURFACE DIFFUSION—Re ON W

A. Diffusion on (123) Planes

The diffusion of rhenium atoms on tungsten (123) planes follows the closely packed atomic channels. The motion is in general symmetric random walks with two reflecting boundaries.[3] The separations between two successive positions of an adatom are found to be integer multiples of a shortest distance. Within 0.5-Å accuracy this shortest distance is found to be equal to 2.74 Å, the nearest-neighbor distance of the substrate lattice. The (123) plane atomic-row separation was used for a calibration of the magnification of the images. The diffusion is thus established to be discrete with a jumping distance of 2.74 Å as originally assumed by Ehrlich and Hudda.[3] In Fig. 1, we give an example of a single-atom one-dimensional discrete random walks. At 332 K, no loss of the Re atom occurred. At 364 K, the Re escaped from the surface channel during the third heating cycle. After the escape, the field-ion micrograph clearly showed an increment of one atom at one end of one of the atomic rows forming the migrating channel.

Exact statistical analysis of the one-dimensional diffusion is possible as shown in Appendix A. It is, however, easier to use the approximate equation given by Ehrlich[9] for data analysis:

$$\langle\langle (\Delta m)^2 \rangle\rangle \approx N[1 - (4/3M)(2N/\pi)^{1/2}] \quad \text{for } 1 \ll N \ll \tfrac{1}{10}M^2 , \quad (1)$$

where Δm is the number of steps displaced in a heating cycle, M is the total number of discrete steps within the boundaries, and N is the number of jumps executed by the atom in a heating cycle. Equation (1) has a maximum mean-square displacement of $\frac{1}{24}\pi M^2$ at $N = \frac{1}{8}\pi M^2$, which is slightly smaller than the exact value of $\frac{1}{6}M^2$. The total number of jumps has been established[3] to be

$$N \approx \tau(kT/h)\, e^{-E_d/kT} , \quad (2)$$

where τ is the heating time and E_d is the activation energy for surface diffusion. The data shown have a mean-square displacement of 30, which gives an N of 52 and $E_d = 0.88$ eV. This agrees with the results given by Bassett and Parsley.[5] It is noted that $N = 52$ exceeds the range where Eq. (1) is accurate. Fortunately, E_d depends on logarithm of N and is rather insensitive to N.

The potential barrier height E_b of the reflecting boundaries can also be estimated. Assuming that

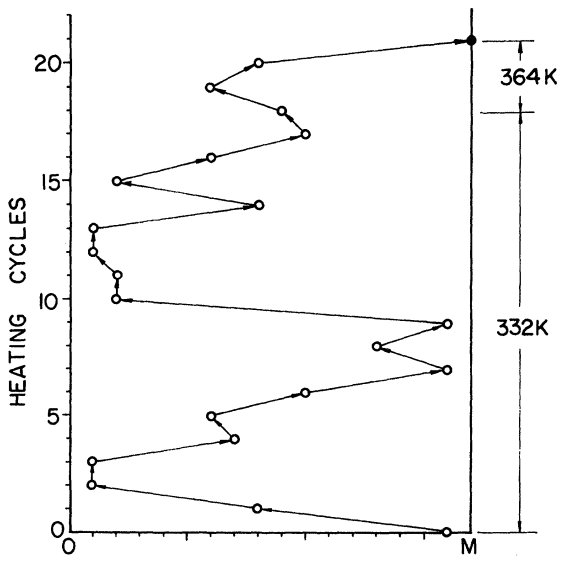

FIG. 1. One-dimensional discrete random walks of a Re atom on a W (123) plane. The diffusion is along a surface channel. Each jumping step is 2.74 Å, and the channel has a total of 17 steps.

at a temperature T' it takes a total of time τ' to escape from the migrating channel, E_b is then given approximately by

$$M/2\sqrt{N} \simeq e^{-E_b/kT}, \tag{3a}$$

$$E_b \approx 2.303kT'\log_{10}\left(\frac{2(\tau' kT'/h)^{1/2}}{M}\right) - \frac{E_d}{2}. \tag{3b}$$

From the data shown, we find $E_b = 0.052$ eV. The activation energy for overcoming the boundary from a surface site at the plane edge is $E_b + E_d = 0.932$ eV. Contrary to what one might expect, the reflecting-potential-barrier height is relatively low.

B. Diffusion on (110) Planes

It is quite reasonable to assume that in the absence of a field, an adatom sits in a surface site rather than on a lattice site because the latter site is a saddle point. It is also assumed that the surface diffusion is along surface channels. There are three paths an adatom can jump over to a neighbor surface site. One of the paths involves jumping over a lattice site and the other two paths involve jumping over between two atoms in a closely packed atomic row. The potential barrier heights are, respectively, represented by E_1 and E_2. They can be determined experimentally from the components of mean-square displacements in two orthogonal directions. For example, one may choose $[\bar{1}10]$ as Y axis and $[00\bar{1}]$ as X axis. Then

$$\langle X^2\rangle = \tau \sum_{j=1}^{z} \nu_j x_j^2, \tag{4a}$$

$$\langle Y^2\rangle = \tau \sum_{j=1}^{z} \nu_j y_j^2, \tag{4b}$$

and

$$\langle R^2\rangle = \tau \sum_{j=1}^{z} \nu_j (x_j^2 + y_j^2). \tag{4c}$$

The summation is over all surrounding neighbor surface sites, and ν_j is the effective jumping frequency to the jth surface site. The three paths discussed will lead to three surface sites with their coordinates given by

$$\begin{aligned} x_1 &= 0, & y_1 &= \tfrac{1}{4}\sqrt{2}a; \\ x_2 &= \tfrac{1}{2}a, & y_2 &= -\tfrac{1}{4}\sqrt{2}a; \\ x_3 &= -\tfrac{1}{2}a, & y_3 &= -\tfrac{1}{4}\sqrt{2}a; \end{aligned} \tag{5}$$

where a is the lattice constant. The effective jumping frequencies are given by

$$\nu_1 \simeq (kT/3h)\, e^{-E_1/kT} \tag{6a}$$

and

$$\nu_2 = \nu_3 \simeq (kT/3h)\, e^{-E_2/kT}. \tag{6b}$$

With a little manipulation, one finds

$$E = 2.303kT\log_{10}\frac{\tau kTa^2}{24h(\langle Y^2\rangle - 1/2\langle X^2\rangle)}, \tag{7a}$$

$$E = 2.303kT\log_{10}\frac{\tau kTa^2}{6h\langle X^2\rangle}. \tag{7b}$$

We have neglected the boundary effect in the analysis. In the temperature range where our data are obtained, the boundary effect is insignificant, as 100% inaccuracy in $\langle R^2\rangle$ introduces an error in the energy of only $0.7kT$, or less than 0.02 eV. At 364 K, from a total of 17 heating cycles with a single Re atom as shown in Fig. 2 we obtain $\langle X^2\rangle = 107$ Å^2 and $\langle Y^2\rangle = 224$ Å^2. They then give

$$E_1 = 0.88 \text{ eV}$$

and

$$E_2 = 0.95 \text{ eV}.$$

Both the energies are slightly lower than the aver-

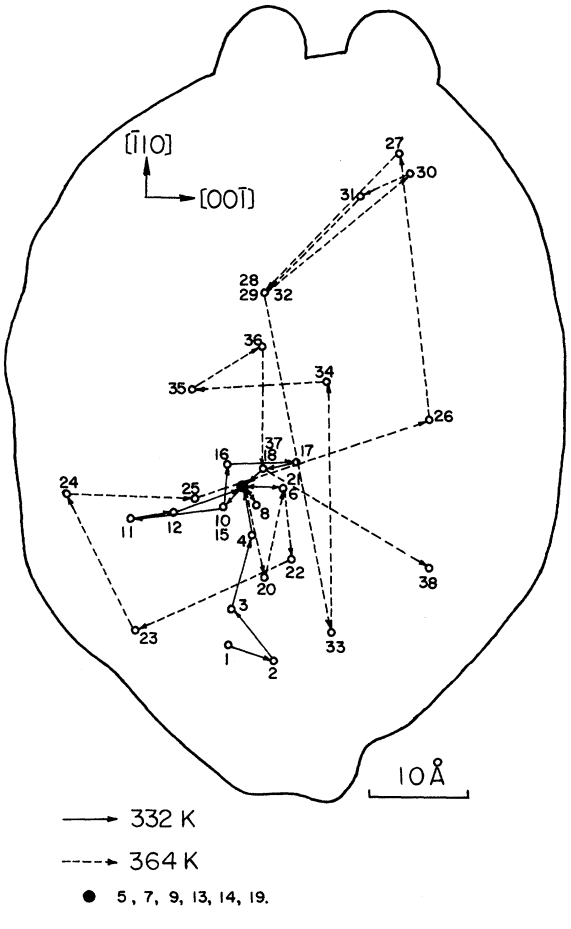

FIG. 2. Two-dimensional random walks of a Re atom on a W (110) plane. The vectors connecting two successive positions of the Re atom are displacement vectors rather than diffusion paths. The dark dotted position is where a surface-potential trap is located.

age activation energy obtained by Bassett and Parsley.[5]

C. Potential Traps on Surfaces

In the course of our single-atom-diffusion experiments, it was found that at lower temperatures the diffusing atom was often trapped in a surface site and could no longer move at the original heating temperature. In some cases we found the diffusing atom to come to a small region more often than that expected from unrestricted random walks. These observations indicate an existence of localized potential traps on surfaces which otherwise appear to be perfectly regular in the FIM images. Figure 2 shows clearly that the dark dotted site is a potential trap. The traps are probably caused by some lattice defects or impurities on or underneath the diffusion planes. No effort was made to uncover them in our experiments. The additional binding energy of the traps can be estimated from a method discussed in Appendix B. Assuming that our resolving capability is 0.5 Å as discussed in Sec. II, by substituting the data shown in Fig. 2 into Eq. (B12) in Appendix B, we obtain

$$\Delta E_t = 0.14 \text{ eV}.$$

The potential traps are relatively weak when compared with the surface binding energy (several eV) or with the activation energy of surface diffusion (~ 1 eV). However, they may play some roles in atomic processes on surfaces.

IV. INDIVIDUAL ATOMIC INTERACTIONS

A. Tungsten-Tungsten Interactions

When more than one tungsten atom is deposited on a W(110) plane, it takes only a few heating cycles around room temperature for them to combine into a cluster. As the probability that three W atoms encounter each other at the same time is small, formation of large clusters is usually achieved by combinations of diatomic clusters or successive capturing of individual atoms. The clusters have definite structures at certain temperatures as will be discussed in Sec. V. The interesting thing is that only one configuration for diatomic clusters has ever been observed below 390 K. The two W atoms, both sitting in a surface site, are always separated by the nearest-neighbor distance of 2.74 Å. The second closest structure one can conceive of, where both atoms sit on a surface site, has an interatomic distance of 3.14 Å. The fact that no such configuration has ever been observed in ~ 100 clusters indicates that the interaction potential-energy difference

$$E_2(2.74 \text{ Å}) - E_2(3.14 \text{ Å}) > 2.303kT \log_{10}(100)$$

$$= 0.15 \text{ eV}.$$

It is also noticed that the diatomic clusters start to dissociate at 390 K. The binding energy is therefore given by

$$E(2.74 \text{ Å}) \approx 2.303kT \log_{10}(2kT/h) = 1.02 \text{ eV}.$$

Both results are consistent with what one may expect from the atomic interaction potentials derived from bulk properties of tungsten with the specific assumption that the atomic interactions are pairwise additive.[10–13] However, it is also noticed that the multiatomic clusters up to six atoms dissociate below 490 K, or $E_6 \lesssim 1.29$ eV. This clearly shows the failure of the pairwise additive assumption in dealing with the binding energies of surface atoms.[3–6,13] While the W-W interaction potential seems to be quite short ranged on W (110) planes, it is not the case on (112) planes. It is often observed that two W atoms in neighboring (112) atomic rows migrate together up to 330 K. Their bond length changes occasionally from 4.47 to 5.24 Å. The stability[8] of the clusters gives a binding energy of 0.56 eV at 5.24 Å. The frequency of observing 5.24-Å bonds is approximately the same as that of observing 4.47-Å bonds. Their binding strength cannot differ more than $kT \approx 40$ meV. Thus the atomic potential of two W atoms on (112) planes seems to be very long ranged. The interatomic potential depends, therefore, on substrate structures. Figure 3 gives an example of

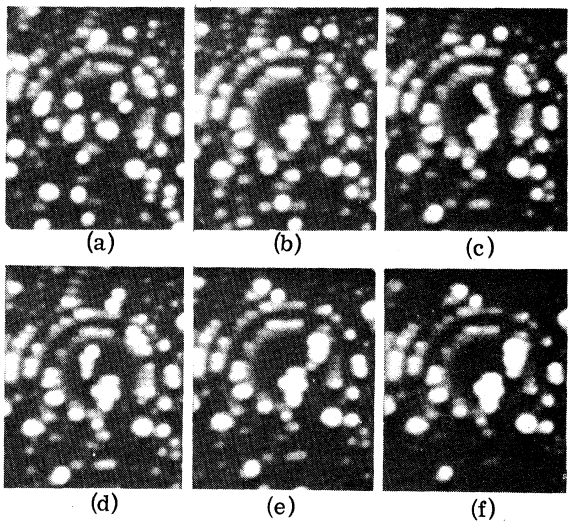

FIG. 3. Ten W atoms have been deposited on a field evaporated W (112) plane as shown in (a). After heating to 300 K for one cycle, six of them combined into W_6 cluster and the other four formed a chainlike W_4 cluster as shown in (b). (c)–(f) show the new locations of the W_4 after each heating cycle at 300 K. The bond lengths in the W_4 cluster changed occasionally from 4.47 to 5.24 Å. The W_6 cluster did not move at 300 K.

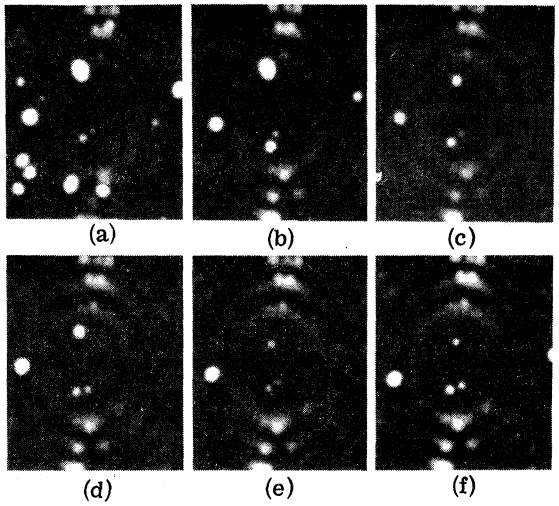

FIG. 4. Surface migration of three Re atoms on a W (110) plane at 315 K. Two of them migrated together with a bond length of approximately 7.5 Å.

a surface migration of 4 atom clusters on a (112) plane.

B. Rhenium-Rhenium Interactions

On W (112) planes, interaction between two rhenium atoms is quite similar to that between two tungsten atoms. On W (110) planes, the situation changes completely. In the 320–390-K range, no stable cluster of any form or even an atomic separation less than a few Å has been observed. In many cases, we deliberately deposited several Re atoms on a (110) plane. After tens of heating cycles, they are still widely separated. The observations indicate an existence of a repulsive potential between two Re atoms. Above 390 K, the potential barrier can be overcome and clusters can be formed. Clusters with more than 3 atoms are found to be stable with respect to reorientation and surface diffusion as will be shown in Sec. V. Diatomic clusters of bond length 2.74 Å are observed but are not stable, suggesting a bond strength of less than 1 eV. Below 320 K, very loosely bound diatomic clusters of bond length ~7 Å as shown in Fig. 4 can be observed. Before our trying to establish the last statement, we will first discuss the consequences of our observations. We have identified two minima, one of ~1 eV at 2.74 Å separation and one of less than 0.8 eV at ~7.2 Å separation, and a relatively weak maximum in between the minima in the interatomic potential of two Re atoms on W (110) planes. This seems to suggest an oscillatory structure in the interatomic potential of two Re atoms similar to the well-known Friedel oscillation.[14,15]

To establish the existence of the second minimum, the field-ion micrographs with three rhenium atoms on a W (110) plane and their maps are shown in Figs. 4 and 5. At 315 K, the atoms *A*, *B*, and *C* have, respectively, mean-square displacements of 15.8, 9.6, and 23 Å^2. According to the analysis given in Appendix C, the mean square in the variations of the two particle separations should be equal to the sum of the mean-square displacements of the two particles, provided that they are executing random walks. For atoms *A* and *B*, the mean-square variation should be 25.4 Å^2. The observed value is only 0.62 Å, almost the limit of our resolving capability. Thus the two atoms are bound together. From its stability at 315 K, its binding energy is estimated to be 0.8 eV. The equilibrium separation is found to be ~7.2 Å from two series of observations. It is interesting to note that the *AB* bond was broken when atom *B* fell into a potential trap. *B* atom escaped from the trap only when the heating temperature was raised to 332 K.

C. Tungsten-Rhenium Interactions

Only preliminary data are available for tungsten-rhenium interactions. On tungsten (112) planes,

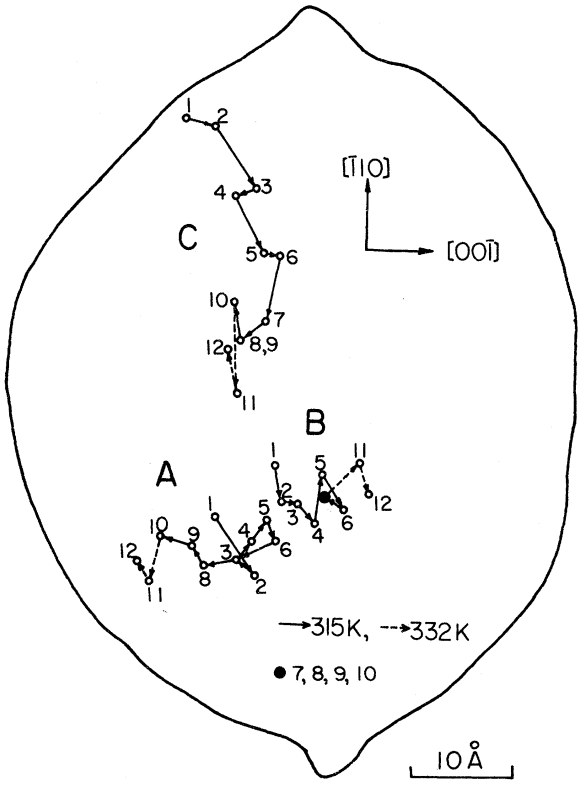

FIG. 5. A map for the three Re atoms shown in Fig. 4. Atoms *A* and *B* migrated together until *B* fell into a potential trap. *B* started to move again only when the heating temperature was raised to 332 K.

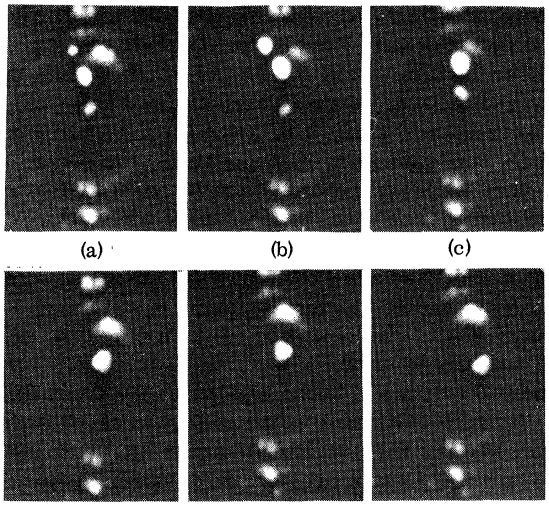

FIG. 6. A W_2 cluster (the dim-image spot) migrated to combine with a Re atom at 332 K. Reorientation of W_2Re clusters can occur even at 332 K. However, noticeable surface migration occurs only above 380 K. The W_2Re images as shown in (d) and (f) have a structure corresponding to *E* in Fig. 8. The image in (e) probably has a structure corresponding to *D* in Fig. 8.

they are quite similar to tungsten-tungsten interactions. When a rhenium atom and a tungsten atom are in two neighboring channels, they may migrate together. Their bond strength is however weaker; thus dissociation occurs frequently even well below 330 K. When a Re and a W are in the same channel, they combine easily to form a cluster of bond length 2.74 Å. The mobility of the latter kind of cluster is very much smaller than that of the former kind. On the (110) plane, similar to two rhenium atoms, no stable WRe cluster is observed below 332 K. A rhenium atom can combine readily with a tungsten diatomic cluster as shown in Fig. 6. The W_2Re clusters are stable up to 460 K. Since there is no stable rhenium diatomic cluster of 2.74-Å bond length, two Re and one W will not combine to form a WRe_2 cluster. The probability of three-atom collisions is much smaller than two-atom collisions and the nonobservation of WRe_2 clusters may simply indicate this fact rather than the instability of the WRe_2 cluster.

Although only limited data are available on W-Re interactions, our work indicates a possibility of investigating initial stages of alloying using the FIM. The metals of interest in the alloying process usually have a low evaporation field. Imaging gases such as neon or argon are more suitable and an image intensification with a channel plate or an external image intensifier is mandatory. We also propose here to study the surface-diffusion process, as well as the initial stage of alloying using room-temperature field-ion microscopy.[16,17] With ultrahigh-vacuum techniques and channel plates easily available now, one can observe the surface diffusion of a single atom, as well as its interactions with other atoms continuously. At room temperature, the FIM has a resolution of ~ 5 Å and thus cannot resolve lattice atoms. However, it is known that individual atoms on a large plane such as (110) of tungsten can be identified.[1]

V. CLUSTER STRUCTURES

Although, as pointed out before, we can pinpoint the position of a single atom to within ~ 0.5 Å, when more than two atoms are close together, their image points no longer appear to be circular and their positions can no longer be accurately determined. With a resolution (the ability to image two atoms separately) of about 3 Å of the FIM, it is difficult to determine the exact structure of clusters without some degree of speculation. The following assumptions will be made for relating the proposed cluster structures to the FIM images: (i) The proposed structures should have the same symmetries as the images. (ii) The proposed structures should be consistent with the resolution of the FIM. (iii) Unless contrary to assumptions (i) and (ii), the atoms are assumed to sit in surface sites. If proper surface sites can not be found, lattice sites (saddle points) and other possible sites are considered. With the above assumptions, the images of clusters with less than 6 atoms as well as their proposed structures are shown in Figs. 7–10. It should be noted that because of the symmetries of the substrate lattice, the clusters may have various orientations. Our observations establish the fact that the clusters have definite structures which are then closely related to the substrate atomic arrangements. The equilibrium structures may change with the surface temperature. One of the surprising results of this investigation is that a W_6 cluster changes from a highly symmetric to a rather low symmetric form at a relatively low temperature of 390 K. The total binding energy of the two structures cannot differ more than $6kT \approx 0.2$ eV. This cannot be understood with the idea of pairwise addition of interatomic potentials. The observation thus suggests a collective effect on the cluster binding energy by all the atoms involved.

The question arises whether the images we observed represent real cluster structures. Indeed, the large polarizability of adatoms will cause them to repel each other in an electric field when they sit side by side. The fact that many of our observed low-temperature equilibrium structures have closest possible bonds shows that the bond strength is enough to resist a break-off by the

imaging field. The less closely bound, higher-temperature form observed must, therefore, represent the real equilibrium structure.

Since the equilibrium cluster structures are so sensitive to surface temperatures, it is quite natural to expect a thermal atomic rearrangement of surfaces. No real effort was made in investigating this process. However, we did observe some surface atomic rearrangements due to the thermal effect alone as shown in Fig. 11. As no systematic study has been done yet, no analysis will be given here.

VI. SUMMARIES

It is shown that using the field-ion microscope, it is possible to investigate the interactions between individual atoms on metal surfaces. The resolving capability of the FIM on the successive locations of a migrating surface atom is much better than the resolution of the microscope. Surface migration of a single rhenium atom on tungsten (123) planes is established to be discrete jumps of 2.74 Å as originally assumed by Ehrlich and Hudda. Surface diffusion on tungsten (110) planes

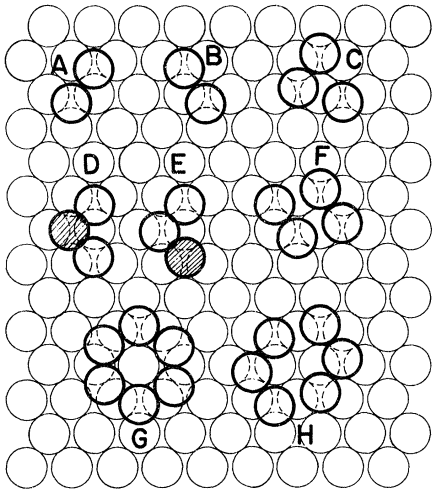

FIG. 8. Proposed structures for multiatomic tungsten and tungsten-rhenium clusters.

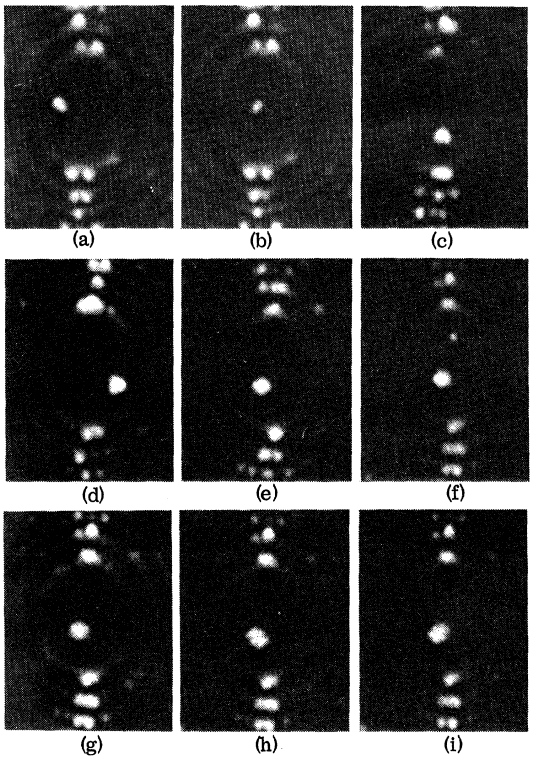

FIG. 7. Tungsten multiatomic clusters. (a) and (b) show images of a W_2 cluster in two orientations. W_3 cluster images are shown in (c) and (d), and a W_4 image is shown in (e). In (f), one sees the images of a W_5 cluster and a single W atom. The low-temperature (< 390 K) W_6 cluster image is shown in (g), and (h) and (i) show the same W_6 above 390 K. Reorientation of the high-temperature W_6 cluster from (h) to (i) configurations occurred around 450 K. Above 460 K, the W_6 dissociated. The structures for clusters shown in (a)–(e), (g), and (h) or (i) are believed to be, respectively, given by *A*–*D* and *F*–*H* of Fig. 8. The W_5 shown in (f) has an image shape very similar to a W_4. It is, therefore, difficult to figure out the W_5 structure.

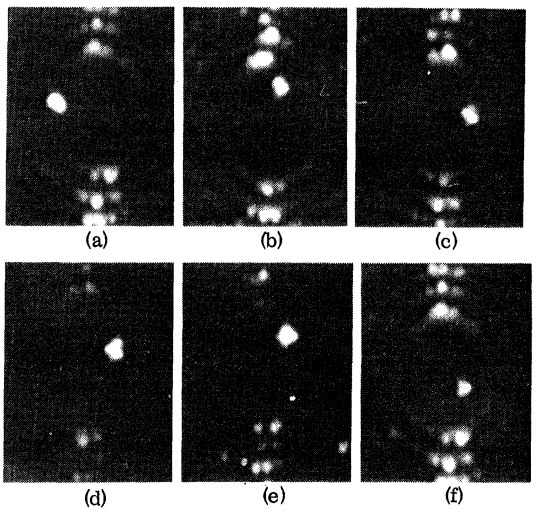

FIG. 9. Rhenium multiatomic clusters. A Re_2 with a bond length of 2.74 Å is shown in (a). A Re_3 is shown in (b). Various forms of Re_4 are shown in (c)–(f). All the multiatomic rhenium clusters shown here can only be formed above 400 K. Re_4 clusters exhibit many equilibrium structures at the same temperature. Restructuring occurs frequently. One rather mysterious fact is that the individual atoms in rhenium clusters vary widely in image intensities. This seems to indicate a specific atomic electronic charge redistribution for each cluster configuration.

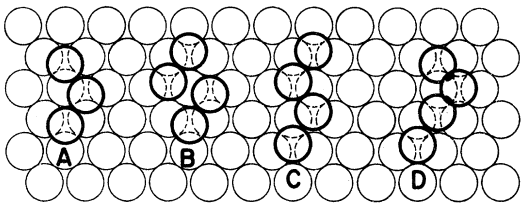

FIG. 10. Proposed structures for Re_3 and Re_4 clusters. Configuration *A* corresponds to (b) of Fig. 9. *B*–*D* correspond, respectively, to (c), (d), and (f) of the same figure. (e) of Fig. 9 has a structure corresponding to configuration *F* of Fig. 8.

is along surface channels by overcoming two potential barriers. The barrier heights can be obtained by evaluating the X and Y components of the mean-square displacements. Many potential traps of approximately 0.14 eV are found on crystal planes which otherwise appeared to be perfectly regular in the FIM images.

To investigate the atomic interactions between surface atoms, one can deposit a desired number of various kinds of atoms on a surface plane, then study their behavior at various temperatures. It is found that interatomic potentials between surface atoms depend very much on the substrate plane structure. While tungsten atoms are readily combined to form multiatomic clusters at low temperatures, rhenium atoms repel each other. However, a weakly bound Re-Re of length ~ 7.2 Å can be observed below 320 K. At higher temperatures, the repulsive barrier can be overcome and clusters with shorter bond lengths can be formed. The observation suggests a possible oscillatory structure of the interatomic potential similar to the Friedel oscillation in solids.

Based on a few reasonable assumptions, some equilibrium cluster structures are proposed which are consistent with the observed FIM images. The equilibrium cluster structures are found to be related to substrate structures and also are found to be very sensitive to surface temperatures. From this observation, it is not unexpected that some forms of surface rearrangement may occur on crystal planes at high temperatures.

Although our data on tungsten-rhenium interaction are only preliminary, the possibility of studying initial stages of alloying using the FIM has now been demonstrated. We also suggest here the possibility of continuously observing a single atom migration on a surface plane and its interaction with other atoms with a room-temperature FIM.

Note added in proof. The last suggestion has now been successfully carried out. Using a room-temperature FIM, we have succeeded in seeing individual atoms creeping on surfaces.[18] From the speed of the atomic movements, the polarizability of the surface atoms can be obtained.

ACKNOWLEDGMENTS

The author wishes to express his sincere gratitude to Professor Erwin W. Müller for his encouragement, advice, and interest in this work. The author also wishes to thank G. L. Fowler for his technical assistance.

APPENDIX A: ONE-DIMENSIONAL DISCRETE RANDOM WALKS

We discuss briefly here the one-dimensional, unrestricted, discrete, random walks with two reflecting boundaries.[19] Let the reflecting boundaries be at 0 and M. The original position of the atom is at m_i. Then the probability that after N jumps the particle is found at m_j is given by the method of images[20] to be

$$W_{m_j,N}(m_i) = \sum_n [U_{2nM+m_j,N}(m_i) + U_{2nM-m_j,N}(m_i)], \quad \text{(A1)}$$

where

$$U_{m_j,N}(m_i) = \frac{N!}{[1/2(N+m_j-m_i)]\,![1/2(N-m_j+m_i)]!}\left(\frac{1}{2}\right)^N. \quad \text{(A2)}$$

We have assumed that N and $(m_j - m_i)$ have the same parity. The summation n is over all integers such that the total number of jumps is equal

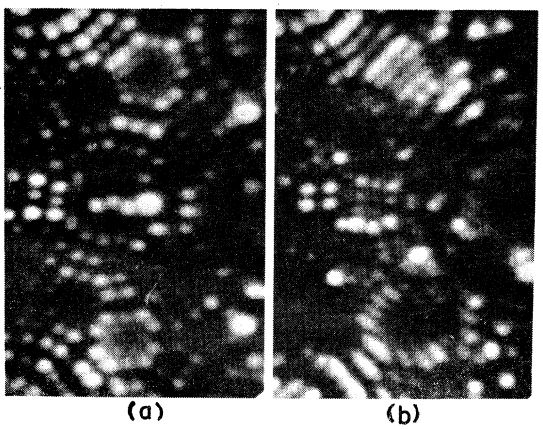

FIG. 11. (a) A portion of a field-evaporated end form of a tungsten tip showing a (130) plane in the middle and two {141} planes in the upper and the lower parts. This surface has already been heated to ~450 K for 5 min. Some surface atomic rearrangements can be noticed. On the top {141} plane, 3 atoms have moved out from the center of the plane to form closely peaked atomic rows on the same plane. (b) The same surface after heating to ~500 K for 5 min. A superlattice structure is now formed at the (130) plane. A complete atomic rearrangement also occurred on the two {141} planes.

to or less than N, or equivalently the denominators of the U's in Eq. (A1) are greater than or equal to 0. For large N and $N \gg |m_j - m_i|$

$$U_{m_j,N}(m_i) \approx (2/\pi N)^{1/2}\, e^{-(m_j-m_i)^2/2N} . \tag{A3}$$

For $N \gg M$

$$W_{m_j,N}(m_i) \approx \sum_{n=-\infty}^{\infty} [U_{2nM+m_j,N}(m_i) + U_{2nM-m_j,N}(m_i)] , \tag{A4}$$

where the U's can be approximated by Eq. (A3). The mean-square displacement is given by

$$\langle (\Delta m)^2 \rangle = \frac{1}{M} \sum_{i=0}^{M} \sum_{j=0}^{M} (m_j - m_i)^2 W_{m_j,N}(m_i) . \tag{A5}$$

APPENDIX B: POTENTIAL TRAPS ON METAL SURFACES

We first discuss the case where the atom executes a one-dimensional random walk without a boundary. Suppose that there are a total of p observations with initial positions of the atom at m_i. The probability for the atom to be found at site m_0, where the potential trap is located, is given by

$$\sum_{i=1}^{p} U_{m_i,N}(m_0) , \tag{B1}$$

where

$$N = \langle (\Delta m)^2 \rangle . \tag{B2}$$

To obtain N, one must use the experimental data where no potential trap has been observed. If a total of q captures in site m_0 occurred during the p heating cycles, one has

$$\frac{1}{q} \sum_{i=1}^{p} U_{m_i,N}(m_0) = e^{-\Delta E_t/kT} , \tag{B3}$$

where ΔE_t represents the additional binding energy of the potential trap at m_0. Or,

$$\Delta E_t = 2.303 kT \log_{10}\left((q/\sum_{i=1}^{p} U_{m_i,N}(m_0)\right). \tag{B4}$$

When reflecting boundaries are present, ΔE_t is still given by Eq. (B4) except $U_{m_i,N}(m_0)$ must be replaced by $W_{m_i,N}(m_0$ of Eq. (A1). For nondiscrete one-dimensional random walks without a boundary,

$$\Delta E_t = 2.303 kT \log_{10}\left(q \Big/ \sum_{i=1}^{p} \frac{\Delta x}{(2\pi N l^2)^{1/2}}\; e^{-(x_i - x_0)^2/2Nl^2}\right), \tag{B5}$$

where Δx is the resolution of the instrument. When reflecting boundaries are present at 0 and a,

$$\Delta E_t = 2.303 kT \times \log_{10}\left(q \Big/ \sum_{i=1}^{p} \sum_{n} [U_{2na+x_i,N}(x_0) + U_{2na-x_i,N}(x_0)]\Delta x\right) , \tag{B6}$$

where the summation n is over all integers and

$$U_{x_i,N}(x_0) \approx \frac{1}{(2\pi N l^2)^{1/2}}\, e^{-(x_i-x_0)^2/2Nl^2} ; \tag{B7}$$

l is the jumping distance. For a symmetric two-dimensional random walk on an infinity plane, the usual relation

$$\langle (\Delta r)^2 \rangle = Nl^2$$

still holds. To achieve a distance r in N jumps, the probability density function is given by the Rayleigh distribution[21]

$$W_N(r) \approx \frac{2r}{Nl^2}\, e^{-r2/Nl^2} \text{ for } N \gg 1 . \tag{B8}$$

Equation (B8) satisfies the required normalization condition

$$\int_0^{\infty} W_N(r)\, dr = 1 . \tag{B9}$$

Assuming that the instrumental resolution is ΔR, the probability, after N jumps, that the atom is found within the potential trap region separated from the initial position by r_{10} is

$$\frac{\Delta R}{2\pi r_{i0}}\; \frac{2\, r_{i0}\, \Delta R}{Nl^2}\; e^{-r_{i0}^2/Nl^2} = \frac{(\Delta R)^2}{\pi N l^2}\; e^{-r_{i0}^2/Nl^2} . \tag{B10}$$

If an atom is originally in the potential-trap region then the probability that after N jumps the atom remains inside the region (say a circular area of radius ΔR) is

$$\int_0^{\Delta R} W_N(r)\, dr = 1 - e^{-(\Delta R)^2/Nl^2} . \tag{B11}$$

Thus the equation we are looking for is

$$\Delta E_t \approx 2.303 kT \log_{10}\left(q \Big/ \sum_{i=1}^{p-q} \frac{(\Delta R)^2}{\pi \langle (\Delta r)^2 \rangle}\; e^{-r_{i0}^2/\langle (\Delta r)^2 \rangle} + q[1 - e^{-(\Delta R)^2/\langle (\Delta r)^2 \rangle}]\right) . \tag{B12}$$

APPENDIX C: DISTANCES BETWEEN TWO PARTICLES

Suppose that there are two particles executing two-dimensional random walks on an infinite plane. The displacement vectors for each heating cycle are

$$\vec{R}_A = \sum_{i=1}^{N} \vec{r}_{Ai} , \tag{C1}$$

$$\vec{R}_B = \sum_{i=1}^{N} \vec{r}_{Bi} , \tag{C2}$$

where $\vec{r}_{Ai}$ and $\vec{r}_{Bi}$ are displacement vectors of ith jump for particle A and B, respectively. The mean-square displacement is given by[22]

$$\langle R_A^2 \rangle = \left\langle \left(\sum_{i=1}^{N} \vec{r}_{Ai} \right)^2 \right\rangle$$

$$= \left\langle \sum_{i=1}^{N} r_{Ai}^2 \right\rangle + 2 \left\langle \sum_{i=1}^{N-1} \sum_{j=i+1}^{N} \vec{r}_{Ai} \cdot \vec{r}_{Aj} \right\rangle$$

$$= \sum_{i=1}^{N} \langle r_{Ai}^2 \rangle \,. \qquad \text{(C3)}$$

The cross term vanishes by averaging because of the random nature of the displacements. When discrete jumps of length l are considered, Eq. (C3) reduces immediately to the well-known form $\langle R_A^2 \rangle = Nl^2$. With a few steps the mean-square variation in the displacement vectors of two particles can be shown to be given by

$$\langle (\vec{R}_A - \vec{R}_B)^2 \rangle$$

$$= \left\langle \left(\sum_{i=1}^{N} \vec{r}_{Ai} - \sum_{i=1}^{N} \vec{r}_{Bi} \right)^2 \right\rangle = \langle R_A^2 \rangle + \langle R_B^2 \rangle \,, \qquad \text{(C4)}$$

the sum of the mean-square displacements of the two particles.

*Supported by the National Science Foundation.

[1]E. W. Müller and T. T. Tsong, *Field Ion Microscopy, Principles and Applications* (American Elsevier, New York, 1969).
[2]E. W. Müller, Z. Elektrochem. 61, 43 (1957).
[3]G. Ehrlich and F. G. Hudda, J. Chem. Phys. 44, 1039 (1966).
[4]E. W. Plummer and T. N. Rhodin, J. Chem. Phys. 49, 3479 (1968).
[5]D. W. Bassett and M. J. Parsley, Brit. J. Appl. Phys. 2, 13 (1969); Nature 221, 1046 (1969).
[6]D. W. Bassett, Surface Sci. 21, 181 (1970); 23, 240 (1970).
[7]T. T. Tsong, J. Chem. Phys. 54, 4205 (1971).
[8]T. T. Tsong, J. Chem. Phys. 55, 2884 (1971).
[9]G. Ehrlich, J. Chem. Phys. 44, 1050 (1966).
[10]L. A. Girifalco and V. G. Weizer, Phys. Rev. 114, 687 (1959).
[11]H. E. Neustadter and R. J. Bacigolupi, Surface Sci. 6, 246 (1967).
[12]R. A. Johnson, Phys. Rev. 145, 423 (1966).
[13]G. Ehrlich and C. F. Kirk, J. Chem. Phys. 48, 1465 (1968).
[14]J. Friedel, Nuovo Cimento Suppl. 7, 298 (1958).
[15]See, for example, W. A. Harrison, *Solid State Theory* (McGraw-Hill, New York, 1970).
[16]E. W. Müller and K. Bahadur, Phys. Rev. 99, 1651 (1955).
[17]R. J. Walko and E. W. Müller, Phys. Status Solidi 9, K9 (1970).
[18]T. T. Tsong and R. J. Walko (unpublished).
[19]The basic probability relations can be found in W. Feller, *An Introduction to Probability Theory and Its Application*, 3rd ed. (Wiley, New York, 1967), Vol. 1.
[20]See, for example, S. Chandrasekhar, Rev. Mod. Phys. 15, 1 (1943); p. 369 of Ref. 18 or Ref. 9.
[21]J. W. Strutt Baron Rayleigh, Phil. Mag. 37, 321 (1919).
[22]J. R. Manning, *Diffusion Kinetics for Atoms in Crystals* (Van Nostrand, Princeton, N. J., 1968).

PHYSICAL REVIEW B VOLUME 6, NUMBER 2 15 JULY 1972

Third-Order Elastic Constants of Tin and of a Tin-Indium Alloy*

K. D. Swartz,† W. B. Chua,‡ and C. Elbaum
Department of Physics, Brown University, Providence, Rhode Island 02912
(Received 8 November 1971)

The complete set of 12 third-order elastic constants (TOEC) of white (metallic) tin and a set of 11 of the 12 TOEC of tin containing 0.3 at.% indium were determined from the hydrostatic and uniaxial stress dependence of ultrasonic velocity. The experiments were carried out on single crystals, using the two-specimen interferometric method of measuring velocity changes. In both the pure and the alloyed crystals c_{333} was largest and negative, and only c_{123} was positive. Some of the TOEC for the alloy were found to differ from the corresponding ones for the pure tin by as much as 20%, e.g. (in units of 10^{12} dyn/cm^2), $c_{112(\text{tin})} = -5.83 \pm 0.12$ and $c_{112(\text{alloy})} = -4.82 \pm 0.13$. All the second-order elastic constants were measured for both types of specimens and were found to be the same within the experimental uncertainty of $\approx 0.1\%$.

INTRODUCTION

Crystal anharmonicity determines or affects various properties of solids, for example, thermal expansion, thermal resistivity, and temperature dependence of elastic constants and attenuation of high-frequency waves.

This anharmonicity is usually treated through an expansion of the strain energy of a crystal in terms of finite strains. The coefficients of terms of a given order in this expansion are conveniently defined as the corresponding-order elastic constants. Alternatively, second-, third-, and higher-order elastic constants can be defined as the second-,

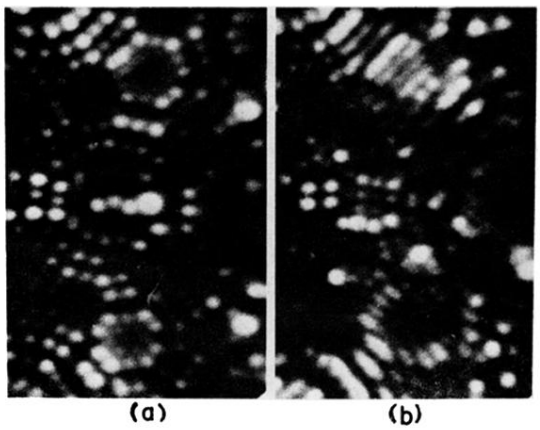

FIG. 11. (a) A portion of a field-evaporated end form of a tungsten tip showing a (130) plane in the middle and two {141} planes in the upper and the lower parts. This surface has already been heated to ~450 K for 5 min. Some surface atomic rearrangements can be noticed. On the top {141} plane, 3 atoms have moved out from the center of the plane to form closely peaked atomic rows on the same plane. (b) The same surface after heating to ~500 K for 5 min. A superlattice structure is now formed at the (130) plane. A complete atomic rearrangement also occurred on the two {141} planes.

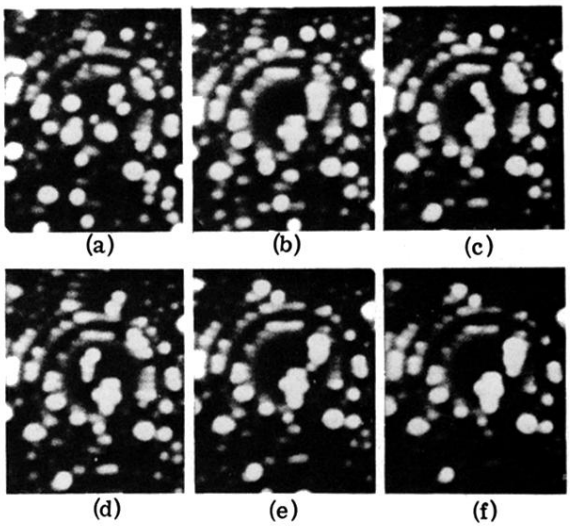

FIG. 3. Ten W atoms have been deposited on a field evaporated W (112) plane as shown in (a). After heating to 300 K for one cycle, six of them combined into W_6 cluster and the other four formed a chainlike W_4 cluster as shown in (b). (c)–(f) show the new locations of the W_4 after each heating cycle at 300 K. The bond lengths in the W_4 cluster changed occasionally from 4.47 to 5.24 Å. The W_6 cluster did not move at 300 K.

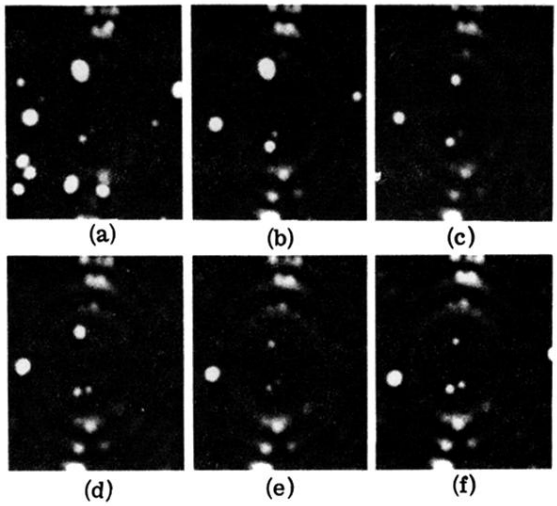

FIG. 4. Surface migration of three Re atoms on a W (110) plane at 315 K. Two of them migrated together with a bond length of approximately 7.5 Å.

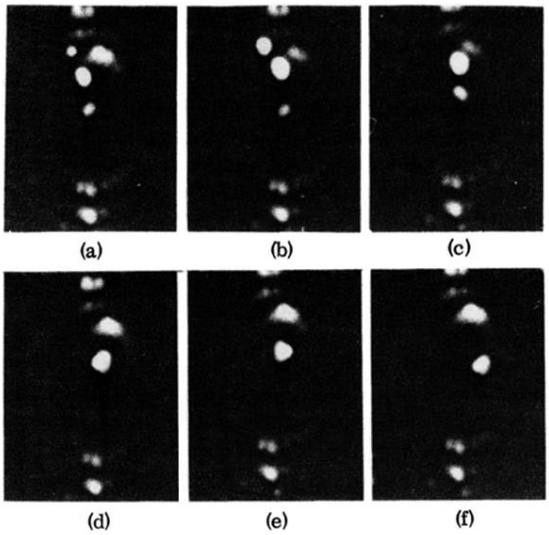

FIG. 6. A W_2 cluster (the dim-image spot) migrated to combine with a Re atom at 332 K. Reorientation of W_2Re clusters can occur even at 332 K. However, noticeable surface migration occurs only above 380 K. The W_2Re images as shown in (d) and (f) have a structure corresponding to *E* in Fig. 8. The image in (e) probably has a structure corresponding to *D* in Fig. 8.

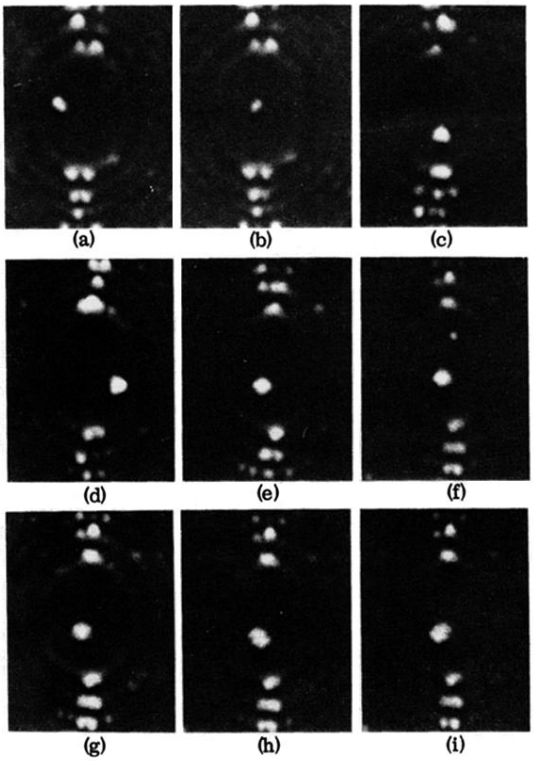

FIG. 7. Tungsten multiatomic clusters. (a) and (b) show images of a W_2 cluster in two orientations. W_3 cluster images are shown in (c) and (d), and a W_4 image is shown in (e). In (f), one sees the images of a W_5 cluster and a single W atom. The low-temperature (< 390 K) W_6 cluster image is shown in (g), and (h) and (i) show the same W_6 above 390 K. Reorientation of the high-temperature W_6 cluster from (h) to (i) configurations occurred around 450 K. Above 460 K, the W_6 dissociated. The structures for clusters shown in (a)–(e), (g), and (h) or (i) are believed to be, respectively, given by *A*–*D* and *F*–*H* of Fig. 8. The W_5 shown in (f) has an image shape very similar to a W_4. It is, therefore, difficult to figure out the W_5 structure.

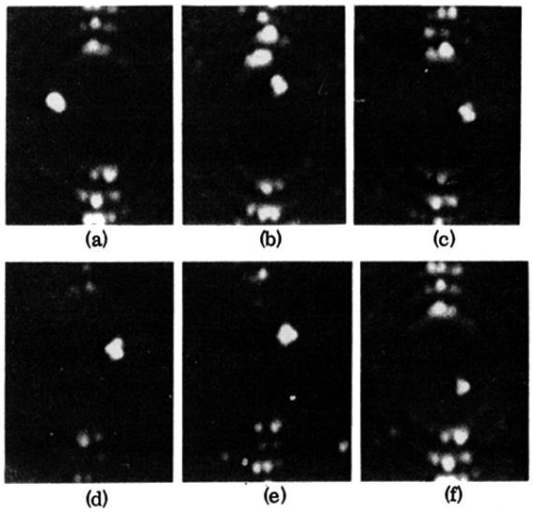

FIG. 9. Rhenium multiatomic clusters. A Re_2 with a bond length of 2.74 Å is shown in (a). A Re_3 is shown in (b). Various forms of Re_4 are shown in (c)–(f). All the multiatomic rhenium clusters shown here can only be formed above 400 K. Re_4 clusters exhibit many equilibrium structures at the same temperature. Restructuring occurs frequently. One rather mysterious fact is that the individual atoms in rhenium clusters vary widely in image intensities. This seems to indicate a specific atomic electronic charge redistribution for each cluster configuration.